JOURNAL OF AEROSOL MEDICINE AND PULMONARY DRUG DELIVERY
Volume 28, Number 5, 2015

Pp. 382–393
DOI: 10.1089/jamp.2014.1168

Surfactant Driven Post-Deposition Spreading of Aerosols on Complex Aqueous Subphases. 1: High Deposition Flux Representative of Aerosol Delivery to Large Airways

Amsul Khanal, PhD,[1,2] Ramankur Sharma, MS,[2,3] Timothy E. Corcoran, PhD,[1,4] Stephen Garoff, PhD,[2,5] Todd M. Przybycien, PhD,[1–3] and Robert D. Tilton, PhD[1–3]

Abstract

Background: Aerosol drug delivery is a viable option for treating diseased airways, but airway obstructions associated with diseases such as cystic fibrosis cause non-uniform drug distribution and limit efficacy. Marangoni stresses produced by surfactant addition to aerosol formulations may enhance delivery uniformity by post-deposition spreading of medications over the airway surface, improving access to poorly ventilated regions. We examine the roles of different variables affecting the maximum post-deposition spreading of a dye (drug mimic).
Methods: Entangled aqueous solutions of either poly(acrylamide) (PA) or porcine gastric mucin (PGM) serve as airway surface liquid (ASL) mimicking subphases for *in vitro* models of aerosol deposition. Measured aerosol deposition fluxes indicate that the experimental delivery conditions are representative of aerosol delivery to the conducting airways. Post-deposition spreading beyond the locale of direct aerosol deposition is tracked by fluorescence microscopy. Aqueous aerosols formulated with either nonionic surfactant (tyloxapol) or fluorosurfactant (FS-3100) are compared with surfactant-free control aerosols.
Results: Significant enhancement of post-deposition spreading is observed with surfactant solutions relative to surfactant-free control solutions, provided the surfactant solution surface tension is less than that of the subphase. Amongst the variables considered—surfactant concentration, aerosol flow-rate, total deposited volume, time of delivery, and total deposited surfactant mass—surfactant mass is the primary predictor of maximum spread distance. This dependence is also observed for solutions deposited as a single, microliter-scale drop with a volume comparable to the total volume of deposited aerosol.
Conclusions: Marangoni stress-assisted spreading after surfactant-laden aerosol deposition at high fluxes on a complex fluid subphase is capable of driving aerosol contents over significantly greater distances compared to surfactant-free controls. Total delivered surfactant mass is the primary determinant of the extent of spreading, suggesting a great potential to extend the reach of aerosolized medication in partially obstructed airways via a purely physical mechanism.

Key words: aerosol, Marangoni spreading, pulmonary drug delivery, surfactant transport

Introduction

Systemic administration of drugs to treat infections associated with cystic fibrosis (CF) requires large doses that may lead to significant unwanted side effects.[1] Given that these infections typically reside in the airways, aerosolized drug delivery is a viable treatment option to minimize circulating drug concentrations in the bloodstream.[1] The presence of highly viscous mucus obstructions in the airways of CF patients creates regions with limited ventilation and

Departments of [1]Biomedical Engineering, [2]Center for Complex Fluids Engineering, [3]Chemical Engineering, and [5]Physics, Carnegie Mellon University, Pittsburgh, Pennsylvania.
[4]Department of Medicine, University of Pittsburgh, Pittsburgh, Pennsylvania.

unusual aerodynamics. These obstructions may hinder aerosol delivery, leading to a heterogeneous distribution of drugs.[2–4]

Current aerosol therapies rely only on aerodynamic mechanisms to disperse and distribute drug inside the lungs after inhalation. Accordingly, aerosols often do not reach infection sites downstream of obstructions, due to limited ventilation and inertial impactions at these obstructions.[2–6] These altered ventilation and deposition patterns frequently leave sites of infections untreated.[2,5–9] Thus, with current aerosol therapies, drugs cannot effectively access all infected regions of the lungs.[1,4,5,7,9] This not only reduces therapeutic efficacy, but may also lead to the development of bacterial drug resistance.[8,10,11] Hence, a need exists to augment aerosol drug delivery to include novel distribution mechanisms that do not rely solely on aerodynamics for distribution in the lungs.

To better access all portions of the lung, we propose the addition of surfactants to aerosol drug formulations to drive spreading after deposition on the airway surface liquid (ASL). Surfactants decrease surface tension by adsorbing to liquid interfaces; gradients in surfactant surface concentrations result in surface tension gradients that can drive convective surface (or ''Marangoni'') flows moving fluid from areas of low surface tension to areas of high surface tension.[12] *In vitro* and *in vivo* studies show that surfactant concentration gradients can be utilized to move exogenous fluid through the lungs.[13–17] Specific surfactants are approved for use in the lungs to treat neonatal respiratory distress syndrome via surfactant replacement therapy (SRT).[18] In SRT, surfactant is delivered in an instilled bolus through an endotracheal tube. The bolus bursts and moves along the airway walls driven by gravity and surface tension gradients to the alveoli where it promotes recruitment.[14,15,18,19] Surfactant instillation has also been used for reopening of fully obstructed lung airways.[14] However, we consider the case where the airways are only partially obstructed, and the inclusion of surfactant in a therapeutic aerosol may serve to drive deposited medication away from sites of heavy deposition, along the ASL and over the mucus obstructions, delivering medication to less ventilated regions in the lungs and increasing dosing uniformity in the airways.

We have previously provided a qualitative, *in vitro* proof of principle for this aerosolized drug dispersal technique using porcine gastric mucin (PGM) solutions and human bronchial epithelial (HBE) cell cultures as ASL mimics.[1] In that study, surfactant-laden aerosols were shown to spread over significantly larger areas than saline controls, but a quantitative determination of the systemic variables that controlled the extent of spreading was not performed.[1] We have also already determined the factors governing the final spread area and the fate of surfactant, solvent (water), and solutes for the deposition of surfactant-laden microliter-scale drops on entangled polymer solution subphases.[20] However, there are important differences between aerosol and single drop deposition that are expected to influence spread area. Medicinal aerosols are $\sim$200x smaller than microliter-scale drops, and their deposition involves interactions of multiple droplets. Therefore, a need exists to address this complexity and the effects of various aerosol delivery variables on the spreading of deposited aerosol droplets.

This study includes a quantitative analysis of the spread area resulting from the deposition of multiple, interacting aerosol droplets containing surfactant, on a subphase that mimics the ASL. We continue the use of our prior model system for *in vitro* measurements: the droplet phase consists of an aqueous solution of a nonionic surfactant, either tyloxapol or a fluorinated nonionic surfactant, with a fluorescent dye, fluorescein, serving as an easily-traced drug mimic; the subphase consists of a chemically simple, entangled aqueous polymer solution, poly(acrylamide) (PA), or an entangled solution of porcine gastric mucin (PGM) to mimic the mucus in the ASL. These model phases together capture the miscibility between aerosol droplet liquids and the ASL. PGM was chosen because of the limited availability of pulmonary mucus, and because it allowed us to establish repeatable surface conditions. We track the movement of the delivered aerosol in an apparatus designed to differentiate deposition and post-deposition spreading. We determine how system variables associated with aerosol delivery, including surfactant concentration, total deposited surfactant mass, total delivered volume, aerosol flow rate, and time of delivery, are predictive of maximum spread area at droplet deposition fluxes that are consistent with inhaled aerosol deposition in the conducting airways (airway generations 0–8, termed ''large airways'' for purposes of this article). The ultimate goal of this research is to develop optimized formulations and delivery techniques that maximize surfactant based spreading after aerosol deposition.

Theory

While there is little guidance from the literature concerning the post-deposition spreading behavior of a field of surfactant-laden aerosol droplets, the spreading of a microliter-scale drop of surfactant solution on solid or liquid subphases is a well-studied problem.[15,19,21,22] As shown in Figure 1, a liquid drop placed on an immiscible liquid subphase will relax to form a lens, with the shape at equilibrium dictated by gravity and the capillary force balance among the three interfacial tensions ($\gamma_{i/j}$) that act on the

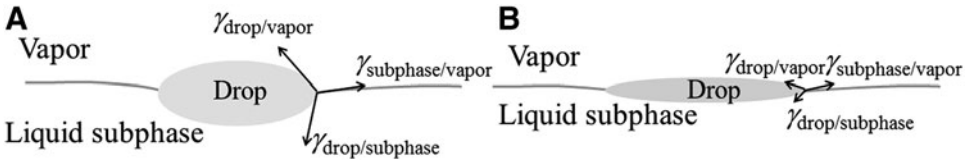

FIG. 1. Interfacial tension forces at equilibrium acting on the three-phase contact line of a liquid drop on a liquid subphase. **(A)** In the absence of surfactant; **(B)** In the presence of surfactant.

three-phase contact line around the drop. Previous studies of individual microliter-scale aqueous drops of water-soluble surfactant solutions indicate that drops spreading on entangled but completely miscible aqueous subphases resemble drops spreading on immiscible subphases.[20,23] On such subphases, quasi-static drops persist for tens of minutes on the subphase surface despite the thermodynamic miscibility of the drop and subphase.[23]

In the case of surfactant-laden drops, surfactant adsorption to the drop/vapor and/or the drop/subphase interface alters the surface tensions at these interfaces. Further, surfactant escapes across the contact line of the drop, lowering the surface tension of the subphase/vapor interface.[23,24] As shown in Figure 1, these altered surface tensions can result in a lens that covers an area larger than that of a surfactant-free drop. In the cases examined here, where the drop and subphase are miscible, the effective surface tension at the drop/subphase interface is very small,[25,26] such that the final area covered by the spread surfactant-laden drop is increased relative to the surfactant-free drop if the initial drop/vapor surface tension is smaller than the initial surface tension of the subphase. During the spreading process, surfactant escape from the drop and adsorption to the expanding drop/subphase and drop/vapor interfaces continually deplete the surfactant concentration in the drop until a new interfacial tension balance among subphase/vapor, drop/vapor, and drop/subphase interfaces is achieved, ultimately limiting the final extent of spreading.[23] We expect that these drop spreading phenomena that were identified with macroscopic microliter drops will also govern individual micrometer-scale (sub-picoliter) aerosol droplet spreading behavior in the absence of interactions with neighboring droplets.

The spreading process itself is dominated by surface tension gradients in the interfaces that form as surfactant moves onto and across the various interfaces. The gradients cause Marangoni stresses that drive fluid flow.[20–23,27] For a single drop, these Marangoni stresses primarily affect the evolution of the drop, while the final surface tension balance dictates the final spread area of the drop, and it assumes a quasi-static shape that persists for tens of minutes.[23] For a field of discrete droplets, these stresses have a more significant impact on the final area covered by the field of droplets that retain their individual identities during the spreading process. This will be described in a companion article by Sharma *et al.*, which contains the results of *in vitro* studies conducted in a different apparatus, at much lower fluxes that are representative of aerosol delivery to small conducting airways.

The inherent many-interacting-droplet nature of aerosol delivery introduces several new timescales in addition to those that characterize the single drop spreading phenomenon. When investigating spreading of an ensemble of aerosol droplets, different timescales associated with the delivery and post-deposition spreading of the droplets have to be considered. $\tau_{\text{monolayer}}$ is the time it takes to deliver a complete monolayer of droplets onto the subphase area under consideration. This provides an upper bound for the time for a fresh droplet to land in an area occupied by previously deposited liquid. $\tau_{\text{spreading}}$ is the time it takes for an individual droplet to complete convective spreading after deposition on a subphase. When there is more than one droplet deposited at distinct locations on the subphase, there are time scales associated with the lateral movement of the centroid of a single droplet which can be termed τ_{lateral}. τ_{lateral} is approximated by the distance between two droplets divided by a characteristic velocity of a moving droplet. If deposited droplets move towards each other and collide, a coalescence event may occur dictated by timescale $\tau_{\text{coalescence}}$. Of these timescales, $\tau_{\text{monolayer}}$ is the one we can most readily control using the system of variables that determine the droplet deposition flux in an aerosol. Its value controls the nature of the fluid body that is spreading on the subphase.

Estimates of aerosol deposition and aerosol deposition flux (liquid volume deposited per area per time) during a nebulizer treatment can be calculated for different airway generations and compared to deposition flux in our experiments. Our calculations utilize airway dimensions from the Weibel model.[28] The probability of aerosol deposition in the airways is dictated by inertial and gravitational mechanisms as a function of branching airway generation.[29] The probability of inertial deposition of aerosol droplets carried by a flowing gas in lung airways depends on the Stokes number (St).[29,30] St compares a droplet's inertia to the viscous drag forces it experiences in the airflow[29]

$$St = \frac{D_p^2 \rho_p u_0}{18 \mu D} \qquad \text{(Eq. 1)}$$

where D_p is the particle diameter, ρ_p is the particle density, u_o is the gas velocity, μ is the gas viscosity, and D is the diameter of the airway. The probability of aerosol deposition via impaction (P_i) increases linearly with St as[29,30]

$$P_i = 1.606St + 0.0023 \qquad \text{(Eq. 2)}$$

This correlation is valid when $\text{St} < 0.62$. Besides inertial deposition, gravitational sedimentation may contribute significantly to aerosol deposition. The probability of aerosol deposition via sedimentation (P_s) can be predicted as[29,31]

$$P_s = \frac{2}{\pi}\left[2\kappa\sqrt{1-\kappa^{2/3}} - \kappa^{1/3}\sqrt{1-\kappa^{2/3}} + \arcsin(\kappa^{1/3})\right] \qquad \text{(Eq. 3)}$$

where

$$\kappa = \frac{3Lv_{settling}}{4\ u_0\ D}\cos\theta \qquad \text{(Eq. 4)}$$

Here, D is the diameter of the airway, L is the length of the airway and $\theta = 38.24°$ is a commonly used tube orientation in lung model sedimentation. The gravitational settling velocity ($v_{settling}$) is given by

$$v_{\text{settling}} = \frac{\rho_{\text{p}} \text{g} D_p^2}{18\mu} \qquad \text{(Eq. 5)}$$

assuming the Cunningham slip correction factor to be 1. P_s is important mainly in the lower airways (higher generation numbers in the Weibel model), where air velocities are small.

Deposition fluxes in lung airways are estimated from the combined deposition probabilities assuming a liquid aerosol inhalation rate of 0.5 mL/min. The two probabilities are

assumed to be additive at the droplet sizes examined in this study. Assuming mono-dispersed droplets with 3 μm diameters ($St < 0.01$ for all relevant air inhalation rates), we calculate the volumetric deposition flux at each airway generation, as shown in Figure 2. The total cross sectional area is the product of the number of branches and their respective cross sectional areas. Aerosol deposition fluxes are estimated for shallow medium and heavy breathing rates, 30, 60, and 90 liters per minute (LPM), respectively.

The predictions represent fluxes encountered at a branch in that particular generation; we take into account the cumulative effect of generation-by-generation depletion via deposition. These predictions do not consider Brownian diffusion as an effective means of deposition as this is only relevant for very small aerosols.[29] We assume that the area of deposition is the projection of the parent airway generation onto the daughter airway generation. A maximum in the deposition flux is observed around the fourth generation for the three inhalation flow rates considered. Total flow area initially decreases from generations 1–3 and then increases from generation 4 through the rest of the airway tree in the Weibel model. Thus, high flow velocities and high rates of impaction would be anticipated in these zones. Deposition fluxes in the large airways, highlighted in gray in Figure 2, range from approximately 0.02 to 0.12 μL/cm^2·sec, while deposition fluxes in the lower airways can be well below 0.01 μL/cm^2·sec.

In this study, the experimental conditions and aerosol deposition fluxes achieved (discussed later) were representative of the larger lung airways (gray region in Fig. 2). The deposition fluxes are such that $\tau_{monolayer}$ is short compared to $\tau_{lateral}$ and possibly $\tau_{coalescence}$. Since individual droplets are not visible in our experiments, we suggest that $\tau_{coalescence}$ is sufficiently fast and we are examining the spreading of a single pool of coalesced aerosol droplets. In our companion article, $\tau_{monolayer}$ is large compared to all the other timescales and individual droplet behavior within the expanding field of droplets, including convective spreading, lateral motion and coalescence, is resolved.

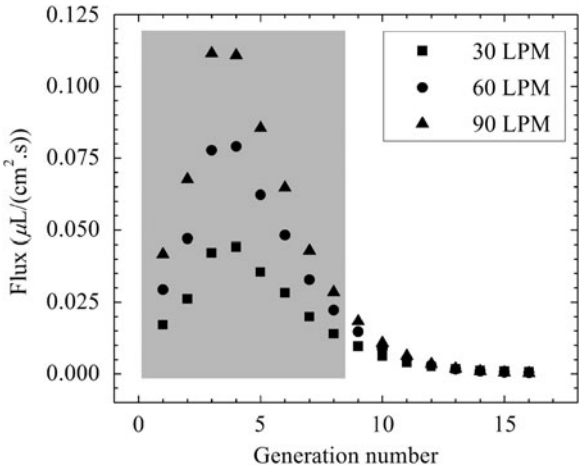

FIG. 2. Estimated aerosol deposition fluxes as a function of airway generation. Fluxes are shown for three different inhalation flow rates (30, 60, and 90 LPM). *Gray box* indicates large airways.

Materials and Methods

Materials

All water was purified to 18 MΩ·cm resistivity, with < 10 ppb total organic carbon (Milli-Q Academic Unit, Millipore Corporation, Billerica, MA). The purified water had a surface tension of 71.5 ± 0.4 mN/m (where the quoted uncertainty here and elsewhere is the standard error of the mean unless otherwise noted) measured using a Wilhelmy pin apparatus (Nima Technology Limited, Coventry, England).

Poly(acrylamide) solution concentrations were above the previously reported 0.45% w/w entanglement concentration.[23] Since it provides a relatively stable surface tension and is an entangled polymer solution, it is used as a simple ASL mimic. PA (CAS# 9003-05-08) of molecular mass 5–6 MDa was purchased from Polysciences (Warrington, PA) and used as received. 1% w/w aqueous PA solutions were prepared in 750 mL of deionized water by adding the powder in increments of 2 g every 2–3 days in a 1 L bottle under nitrogen with continuous gentle mixing on a gyratory shaker (New Brunswick Scientific, Edison, NJ, model G79, speed ''4''). After adding the final 2 g of powder, water was added to bring the total volume to 1 L, and stirring continued for 2–3 more days or until the solution was homogeneous, whichever took longer. The pH was adjusted to 9 with 1 M NaOH, in order to ensure a high quantum yield for the fluorescein dye that is used as a drug mimic and tracer in this study. A high quantum yield of fluorescein dye improves the visualization of post-deposition aerosol spreading.

Although here the aerosol droplets are adjusted to pH 9, pH 7 would be preferred for eventual clinical application to avoid any toxic effects. However, we have found no difference in surface tensions of the surfactant solutions at pH 7, which suggests that their spreading behavior will not vary by changing the pH from 9 to 7. The density of the resulting PA solution was 1.000451 ± 0.000029 g/mL at 23°C, as measured using Anton Paar DMA 500M scanning densimeter (Anton Paar USA Inc, Ashland, VA). The liquid/vapor interfacial tension of the PA solution after pouring a fresh sample was 70.8 ± 0.5 mN/m, which typically decreased by ~ 1–2 mN/m over 5 minutes.

Porcine gastric mucin (PGM; Type II, bound sialic acid ~1% CAS# 84082-64-4) was purchased from Sigma Aldrich. The PGM was stored between 2°–8°C while not in use and was rehydrated with DI water. A 5% w/w solution of PGM was prepared in DI water and was stirred magnetically for ~14 hours, at which point the solution was visually homogeneous. Aliquots of 1 M NaOH solution were then added to the PGM solution to bring it to pH 9. The 5% w/w concentration is above the entanglement concentration of PGM in water, and mimics the ASL mucus to some extent.[20] The prepared PGM solutions were stored between 2°–8°C and used within 4–5 days of preparation. The liquid/vapor interfacial tension of the 5% w/w PGM solution was 38.3 ± 3.5 mN/m, and typically decreased by 2–3 mN/m over 5 min after pouring a fresh sample. PGM solution surface tensions demonstrate complex time-dependencies, likely due to chain dynamics at the solution/vapor interface.

Fluorescein dye (laser grade 99%, CAS# 2321-07-5) was purchased from Fisher Scientific, dissolved at 10 mM in deionized water and adjusted to pH 9 using 1 M NaOH. The

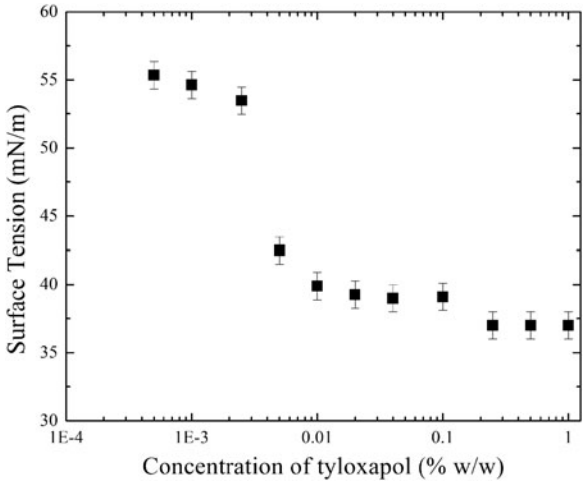

FIG. 3. Surface tension isotherm of tyloxapol in aqueous solution with 10 mM fluorescein.

liquid/vapor interfacial tension and density of the solution were 71.4 ± 0.5 mN/m and 1.001614 ± 0.000033 g/mL, respectively, at 23°C.

The oligomeric nonionic surfactant tyloxapol (CAS #25301-02-04) was purchased from Sigma Aldrich and used as received. The surfactant was dissolved in the fluorescein solution to produce concentrations of 0.1, 0.2, and 0.4% w/w. Wilhelmy pin measurements of the surface tension of these tyloxapol/fluorescein solutions are shown in Figure 3. In accordance with behavior previously reported in the literature, the surface tension isotherm shows two breaks, indicative of the polydispersity of tyloxapol.[32] A decrease in surface tension is observed as the surfactant concentration is increased above 0.001% w/w. The increasingly negative slope observed with increasing surfactant concentration in Figure 3 is characteristic of surfactant solutions. This indicates that 0.1% w/w tyloxapol has a surface tension of 39.1 ± 1.0 mN/m, and the 0.2% w/w and 0.4% w/w tyloxapol solutions have surface tension of 37.0 ± 1.0 mN/m (where the uncertainties in the measurements are instrumental noise). The fluorosurfactant Capstone FS-3100 (DuPont) was used at 1.4% w/w, which is above its critical micelle concentration (CMC) as shown in our companion article, with a surface tension of 17.5 ± 1.0 mN/m (where the quoted uncertainty is instrumental noise).

Experimental methods

Aerosol generation and delivery apparatus. The aerosol deposition and spreading system is illustrated schematically in Figure 4. An ultrasonic nebulizer (Ultra Neb-99, Model 099HD–Devilbiss, Somerset, PA), set at maximum output, was used to aerosolize solutions from a nebulization cup. Two mL of solution was added to the cup for each experiment. The nebulizer output was passed through a series of tubing pieces (Tygon, Saint-Gobain Corporation, purchased from VWR Scientific, Radnor, PA), progressively decreasing in diameter until the aerosol was delivered into the deposition chamber through a 3.8 mm inner diameter glass cannula. The aerosol exiting the cannula was sized in open air by laser diffraction in a parallel set of measurements using a Malvern Mastersizer S (Malvern Instruments, Worcestershire, UK). The aerosol carrier gas was humidified nitrogen heated to approximately 33°C using a respiratory humidifier (MR850JHU, Fisher and Paykel Healthcare Ltd, Auckland, New Zealand). The carrier gas flow rate was set via a flow meter (SSA973 R2, Key Instruments, Trevose, PA) upstream of the nebulizer to either 300 or 450 mL/min. Aerosol size measurement experiments and aerosol spreading experiments were performed separately.

Four mL of the subphase solution was poured into a horizontal square cross-section acrylic tube with inner dimensions $0.26'' \times 0.26'' \times 18''$ (EPlastics, San Diego, CA), with a hole drilled in the center of the tube angled at 15° to admit the cannula tip. The ends of the tube were half covered to contain the subphase solution and also allow for gas to exit the tube. After filling the bottom of the tube with the subphase, the subphase was allowed to level-off to its equilibrium distribution in the tube for ~ 500 sec by placing the tube in a holder specially designed to keep it flat and level, while humidified air was introduced at one end of the tube at 900–1100 mL/min to prevent the subphase surface from drying. Some instances of residual gravity-driven leveling flow of the subphase, after the normal leveling off period, were measured to be on the order of 0.004 cm/sec as observed via movement of a polystyrene bead placed on the subphase. The depth of the subphase for all spreading

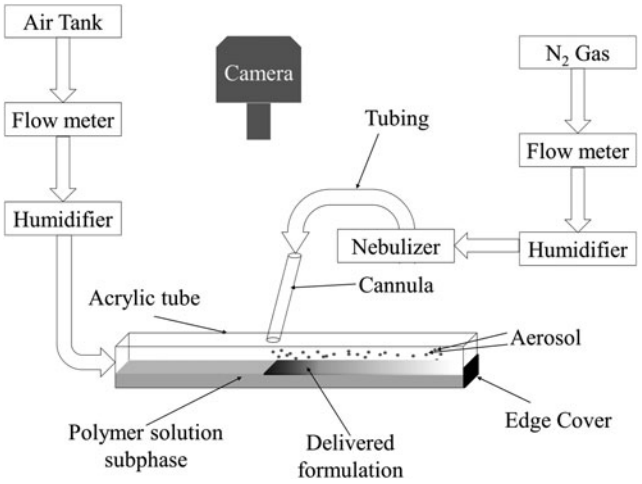

FIG. 4. Schematic of aerosol delivery apparatus. The delivered aerosol (shown as a *gray gradient* on the subphase) is deposited downstream of the cannula due to the bias gas flow. The majority of the delivery occurs close to the cannula. Post-deposition spreading is observed on the subphase upstream of the cannula.

experiments was ~ 0.1 cm. The gravitational parameter ($G = \rho g H^2/\Delta\gamma$)[33] is the ratio of gravity to Marangoni forces, where ρ is subphase density (1000 kg/m^3), g is the gravitational constant (9.8 m/sec^2), H is the subphase depth (0.1 cm), and $\Delta\gamma$ is the subphase surface tension difference before and after surfactant adsorption (on the order of 1 mN/m). In all experiments $G > 1$, suggesting that there is no rupture of the subphase during the spreading process.[33]

Aerosol deposition commenced after the subphase gravitationally leveled off to a constant height throughout the tube after being poured. During deposition, the flow of a humidified air stream passing over the subphase served as a bias gas, driving all nondeposited aerosol out of one end of the tube, through a filter. This made it possible to confine all direct aerosol deposition to a well-defined region of the subphase and, thus, to distinguish between tracer dye deposition and dye spreading after deposition, which moves in the opposite direction of the bias gas flow.

Deposition times were varied between 30–90 sec, so as to achieve different volumes of delivered aerosol. In an effort to identify the factors controlling the extent of post-deposition spreading, we deposited aerosols under varying conditions of surfactant concentration, deposition time, and/or carrier gas flow-rate. The last factor controls droplet delivery rate, and for any given delivery rate, the deposition time and surfactant concentration control the total mass of delivered surfactant. For example, similar surfactant masses would be deposited by delivering a dilute solution for a longer time or a concentrated solution for a shorter time, at the same delivery rate. Maximizing the extent of spreading was the objective, as the goal of developing a self-dispersing aerosolized drug carrier is to provide the most far-reaching and homogeneous distribution of drug possible in the lungs.

Microscopy. The extent of the post-deposition spreading of the delivered aerosol was determined using epi-illumination fluorescence microscopy with a Nikon AZ100 microscope (Nikon Instruments Inc, Melville, NY) equipped with an AZ-Plan Apo 0.5× (NA 0.05/ WD 54 mm) objective and a fluorescence filter cube set (Nikon B-1E) suitable for specimens containing fluorescein. The microscope camera (model DS-QiMc–Nikon) had 0.6× magnification. Images were captured with NIS-Elements Basic Research software and analyzed using NIS-Elements Advanced Research software, both purchased from Nikon Instruments Inc, Melville, NY.

Subphase collection and determination of total deposited dose. The total amount of aerosol deposited was determined by assaying the amount of fluorescein tracer that deposited onto the PA solution subphase. After aerosol deposition and spreading, the subphase was collected by draining and carefully rinsing the tube with 4 mL of DI water to collect all contents. The collected sample's visible absorbance spectrum was recorded in a 1 cm × 1 cm quartz cuvette using a UV-Vis spectrophotometer (Cary 300, Agilent Technologies, Santa Carla, CA). The background water and cuvette absorption were subtracted. Given the inverse dependence of turbidity on the fourth power of the wavelength of the scattered light, a fitted baseline consisting of a quartic fit at wavelengths far from the fluorescein absorbance peak (fitting from 375–405 nm and 550–580 nm), was subtracted from the spectrum to correct for light scattering

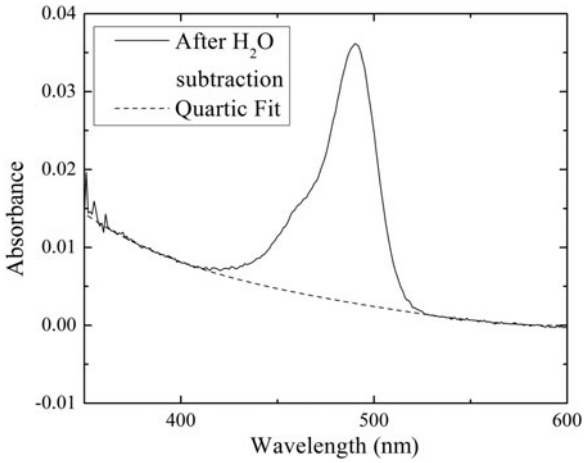

FIG. 5. Representative absorbance spectrum for 1% w/w PA solution at pH 9 with fluorescein after background absorbance subtraction. The fitted quartic baseline representing scattering from the polymer solution is also shown.

from the polymer solution. The fluorescein concentration in the collected sample was calculated from the remaining absorbance at 490 ± 2 nm (Fig. 5). After accounting for diffuse light scattering, fluorescein absorbance in PA solution at pH 9 was well described by the Beer-Lambert Law with a molar extinction coefficient of $(8.5 \pm 0.22) \times 10^5$ M^{-1}cm^{-1}, in accordance with a value of 7.69×10^5 M^{-1}cm^{-1} as reported in literature.[34]

Thus, the concentration of fluorescein deposited in each experiment was determined. Since the volume of the collected sample was known, as was the fluorescein concentration in the aerosolized solution, the total volume of deposited aerosol could be calculated. Furthermore, since the surfactant concentration in solution in the nebulizer was known and we proved (discussed below) that the concentrations of fluorescein and surfactant in the aerosol were the same as they were in the nebulization cup, the total deposited amount of surfactant could be calculated for each experiment.

A possible change in concentration of the surfactant and fluorescein during nebulization was determined by recording absorbance of the collected sample after aerosolization and comparing it with the pre-aerosolized sample. The absorbance values of the fluorescein for the aerosolized and pre-aerosolized samples were similar with a p value of 0.6. Similarly, the absorbance values for the tyloxapol surfactant at 280 nm and FS-3100 at 227 nm for the aerosolized and pre-aerosolized samples were indistinguishable with p values of 0.2 and 0.3, respectively. These results show that there is no change in the concentration of the fluorescein or the surfactant on nebulization. Since the surfactant concentration was unchanged by aerosolization, the surface tension of the aerosolized solutions equals that of the original solution.

Results and Discussion

Aerosol sizing

Table 1 summarizes the delivered aerosol size distributions for each of the solution compositions at two different carrier gas flow rates. All solutions contained 10 mM fluorescein and

Table 1. Aerosol Size Distributions As Function of Tyloxapol Concentrations and Carrier Gas Flow Rates in Aerosol Spreading Experiments

	Carrier gas flow rate			
	450 mL/min		*300 mL/min*	
Tyloxapol concentration (% w/w)	*50^{th} Percentile (μm)*	*10^{th}–90^{th} Percentile (μm)*	*50^{th} Percentile (μm)*	*10^{th}–90^{th} Percentile (μm)*
0	3.2 ± 0.1 [$n=5$]	2.0–5.5	2.8 ± 0.1 [$n=6$]	1.7–4.9
0.1	2.8 ± 0.1 [$n=5$]	1.6–5.0	2.5 ± 0.1 [$n=5$]	1.6–4.2
0.2	3.0 ± 0.2 [$n=8$]	1.7–6.0	2.4 ± 0.1 [$n=3$]	1.4–12.6
0.4	3.2 ± 0.1 [$n=5$]	1.7–6.0	3.3 ± 0.3 [$n=5$]	1.8–8.3

Volume median diameters (50^{th} percentile) are reported along with distribution width (10% and 90% volume diameters); n represents number of experiments performed.

were at pH 9. Reported sizes are volume-weighted median diameters. There was no monotonic dependence of the median droplet size on surfactant concentration. The median aerosol diameters were within the usual range used for clinical inhalation therapies (1–5 μm).

Delivery and movement of aerosol

Tracking movement of delivered aerosol. Figures 6 and 7 show representative deposition experiments where the bias gas flow is from left to right. Figure 6 confirms that the bias gas flow produces a sharp boundary to the region of direct deposition. In the top view shown in Figure 7, the aerosol had been deposited onto the subphase, out of view of the camera system (to the right), and the post-deposition spreading of tracer to the left, shown in black, is evident. Before the end of the delivery period (Fig. 7A and 7B), no fluorescence was detected to the left of the cannula as indicated by the average intensity scans at these times as shown in Figure 7H. At time zero, the aerosol delivery was stopped. As observed in Figure 7C–7G, post-deposition spreading was evident at 10 sec and continued for approximately 10 min after deposition, where in this particular case the spread distance plateaus, as shown in Figure 7I. The parabolic shape of the front indicates a retardation of the spreading of the pool of coalesced droplets along the walls. This is consistent with a convective flow of the tracer solution with a no-slip boundary condition at the walls, rather than diffusion.

For comparisons among different experiments, the position of the tracer dye front was tracked from the initial deposition location along three horizontal lines evenly spaced across the width of the tube. The front was defined as the position where the average intensity exceeded the average baseline value by one standard deviation of the baseline intensity. The front location was used to represent the time-dependent extent of spreading and plotted as a function of time for every experiment. Representative examples are shown in Fig. 7I, where it is evident that the maximum spread distance is different for the surfactant solution and the surfactant-free aerosol ($p < 0.0001$).

Behavior of dye front. As previously noted, for our delivery conditions, more than a monolayer of droplets is rapidly delivered and hence the spreading of individual deposited droplets is not visible. At the magnification required for these experimental conditions, we cannot conclusively determine if the delivered aerosol is a single pool of liquid or an agglomeration of non-coalesced droplets. However, either of these two conditions is consistent with $\tau_{monolayer} < \tau_{lateral}$. For the measured deposited aerosol volumes, subphase area and total time of deposition, we determined that the experimental deposition fluxes were in the range of 0.005–0.078 μL/(cm^2·sec).

These deposition fluxes can be compared to the estimates of airway deposition flux in Figure 2. Assuming monodispersed aerosol particles with diameters 3 μm, the lower bound of experimental fluxes is comparable to aerosol deposition flux in generations 8 and 9 during a 30 LPM inhalation, whereas the upper bound of the experimental deposition fluxes is comparable to deposition flux in generations 3 and 4 during a 60 LPM inhalation. We assume a liquid inhalation rate to be 0.5 mL/min

As discussed earlier, for a microliter-scale drop, a surface tension imbalance at the drop contact line pulls the drop and

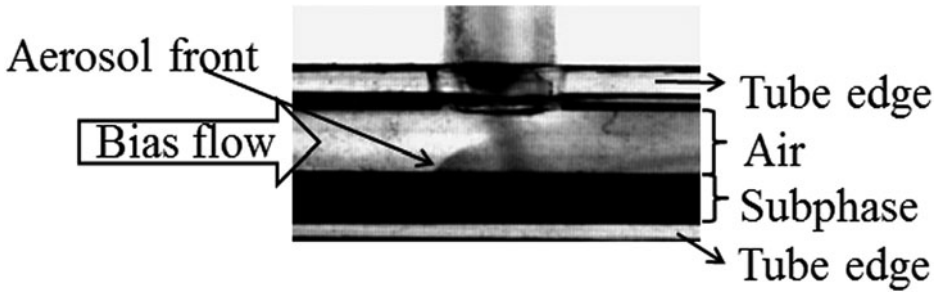

FIG. 6. Side view of aerosol delivery apparatus during a deposition experiment.

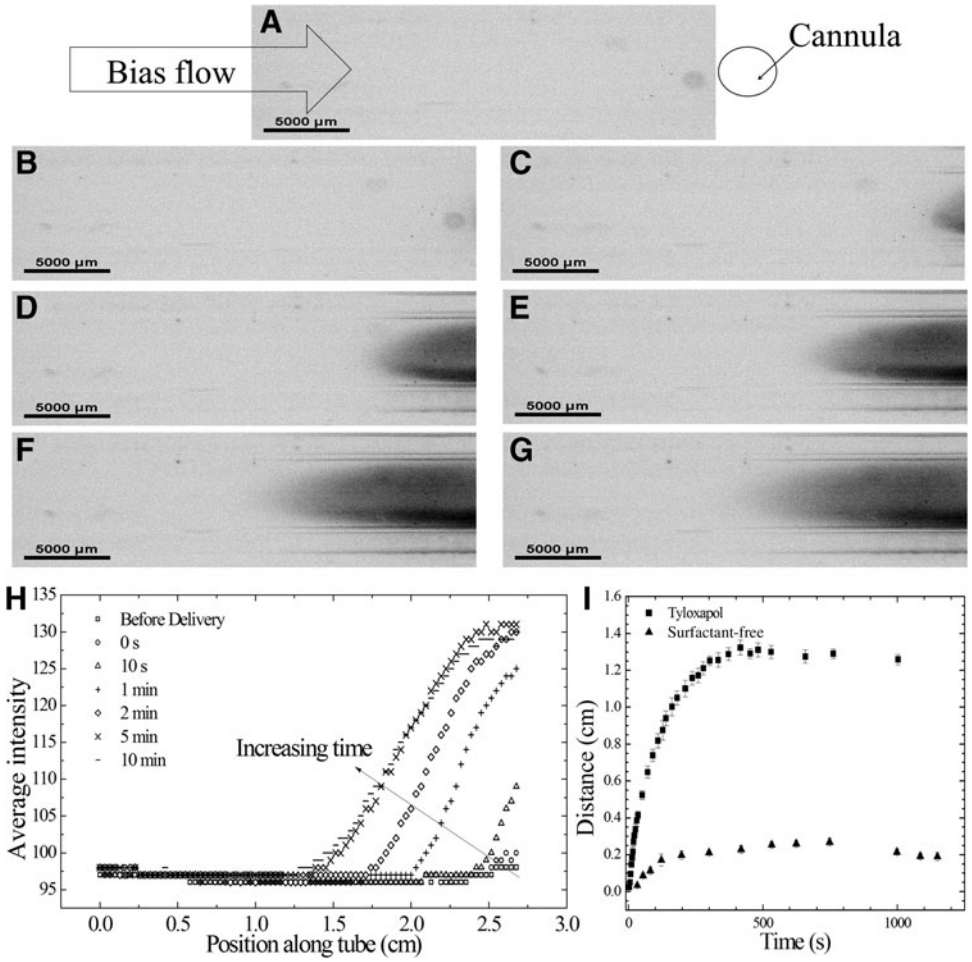

FIG. 7. Representative top-view images of post-deposition spreading along the PA solution subphase with increasing time for aerosolized 0.1% w/w tyloxapol solution delivered at a 300 mL/min carrier gas flow rate. **(A)** Before delivery, **(B)** 0 sec (at the end of delivery), **(C)** 10 sec, **(D)** 1 min, **(E)** 2 min, **(F)** 5 min, and **(G)** 10 min after the end of delivery. *Grayscale figures* were inverted, with the presence of fluorescein tracer dye indicated by *black pixels* to facilitate viewing. **(H)** Image intensity value for spreading dye along the tube averaged across the width of the tube. Every 15th pixel is plotted to make viewing easier. **(I)** Distance moved by tyloxapol aerosol front shown in **(A–G)** and that by surfactant-free fluorescein solution (both with delivered volume $\sim$0.22 μL).

spreads it to cover a larger surface area than surfactant-free solutions of similar volume.[20,23] The post-deposition spreading of microliter-scale drops is driven by the surface tension gradient along the subphase and the resulting Marangoni flow. In aerosol deposition experiments, this force imbalance moves the dye front in the direction of the surfactant free region, allowing for delivered surfactant-containing liquid to cover areas larger than that for the surfactant-free control, as shown in Figure 7I.

Figure 8 shows two qualitatively different behaviors observed in experiments with surfactant-laden aerosols, labeled in the figure as either ''retraction case'' or ''plateau case.'' The plateau case is representative of the great majority of the experiments. The distance traversed by the front typically increased monotonically until plateauing after 5–10 min. Retraction is observed only when the delivered surfactant mass is less than 0.5 μg, and even then, only about 50% of the time. Our observations have also indicated a partial retraction after spreading of a single microliter-scale drop of surfactant solution deposited on an entangled aqueous polymer solution. The phenomenon has been attributed to the difference between the rates of surfactant escape across the drop contact line onto the subphase surface and surfactant desorption into the subphase.[35,36] Apart from this intrinsic process, another extrinsic factor, a slow gravity-driven leveling flow of the viscous subphase, may play a role. This slow leveling off of the subphase may have been important in the low surfactant inventory experiments where spreading front velocities were generally smaller and may have been surpassed by the slow leveling flow. In the small number of experiments where a retraction was observed, we report the maximum extent of spreading as the greatest distance traversed before retraction began.

Controlling factors for maximum spread distances and comparison to single microliter drops. Figure 9 shows that

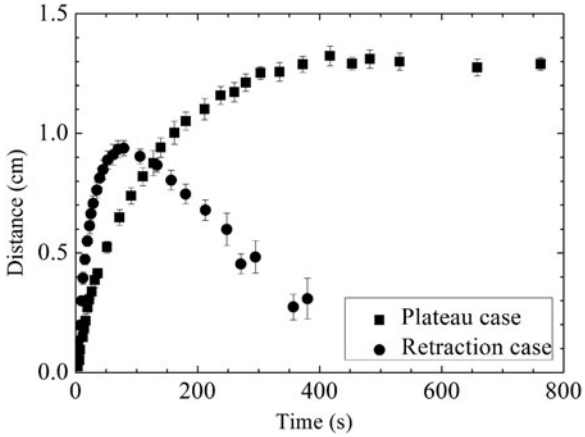

FIG. 8. Spreading of the surfactant front for two representative experiments on a PA solution subphase. Both cases were observed in experiments conducted at a 0.1% w/w tyloxapol concentration and 300 mL/min carrier gas flow rate.

the maximum spread distance increases monotonically with increasing delivered surfactant mass. Different delivered surfactant mass values were obtained by independently varying surfactant concentration, carrier gas flow rate and delivery time. The statistical analysis below indicates that deposited surfactant mass is the primary determinant of the maximum spread distance.

In order to determine relevant variables that are significant for maximum spread distance, multivariable regression analyses were performed on OriginPro 8, taking into consideration the independent variables (surfactant concentration and carrier gas flow rate) and the dependent variables

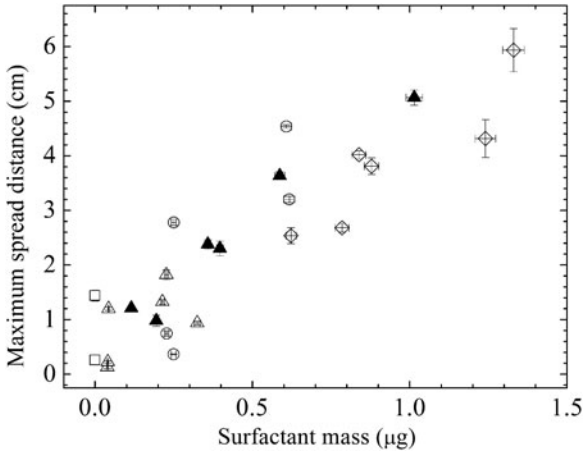

FIG. 9. Maximum spread distance of tyloxapol aerosol as a function of deposited tyloxapol mass when delivered on an entangled PA solution subphase. Symbols indicate different tyloxapol concentrations (□ = 0% w/w, ○ = 0.1% w/w, △ = 0.2% w/w, and ◇ = 0.4% w/w). *Open symbols* indicate carrier gas flow rate of 300 mL/min and *filled symbols* at 450 mL/min. The x-errors are the standard error on the determination of surfactant mass, and the y-errors are measurement errors on distance.

(total delivered volume, surfactant mass, and maximum spread distance). Since total volume delivered was assumed to be dependent on the flow rate and time of delivery, we determined the dependence of the total volume delivered on these two independent variables as well as the product of these variables. The correlation of the delivered volume to these variables was very weak, with no apparent correlation; therefore, we did not perform any backwards elimination to determine the most relevant variables.[37]

Similarly, the dependence of the surfactant mass on each of the three independent variables as well as the product of these three variables was performed. Backwards elimination based on the F-values and adjusted R^2 of the fits determines that the surfactant mass is dependent on the product of the three independent variables. The adjusted R^2 for this fit was 0.67. The dependence of the maximum spread distance on the three independent variables, the product of flow rate and time of delivery, and the product of flow rate, time of delivery, and surfactant concentration was determined via multivariable regression analysis and backwards elimination as in the previous case. The best fit that resulted from the process had an adjusted R^2 of 0.47, and was dependent on the time, flow rate, the product of flow rate and time, and also the product of flow rate, time, and surfactant concentration. Elimination of any of these remaining variables results in a reduced adjusted R^2.

Weighted least squares regressions were performed to determine the dependence of the maximum spread distance on each independent variable as well as the other two dependent variables. These linear regressions determine that the most statistically significant correlation of maximum spread distance was with the surfactant mass (a dependent variable) $R^2 = 0.79$ and $p < 0.0001$. It was also found that surfactant concentration weakly correlated with maximum extent of spreading ($R^2 = 0.46$). The flow rate, delivered volume, and delivery time were uncorrelated with maximum spread extent with R^2 values of 0.01, 0.26, and 0.09 respectively. A linear regression between the volume delivered and surfactant mass determined no correlation (adjusted $R^2 = 0.05$). These different correlations determine that there could be other hidden variables (such as bias flow, cannula entry angle, nebulizer efficiency) that could be affecting the volume and surfactant mass delivered. Since the control for these hidden variables was not ideal, we cannot control *a priori* the volume delivered, yet we do measure it directly with confidence. Since we do have a measurement of the surfactant mass delivered, the strong correlation of the maximum spread distance with delivered surfactant mass is well-supported by the data.

Since the coalescence of the aerosol droplets into a single pool is a possible result at these deposition fluxes, we might expect the deposited aerosol droplet field to behave as if it were coalesced into a microliter-scale drop, where prior work has indicated the controlling role of surfactant mass in extent of spreading.[36] We performed spreading experiments with microliter surfactant-laden drops with different volumes and surfactant concentrations to compare aerosol spreading behavior to that of a single microliter-scale drop in the same apparatus.

Figure 10 indicates a monotonic increase in the maximum extent of spreading with total deposited surfactant mass. Similar to the aerosol experiments, these deposited

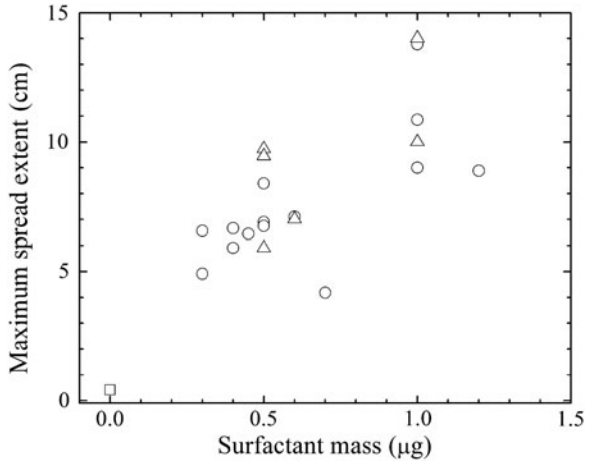

FIG. 10. Maximum spread extent of microliter drops of tyloxapol solutions at different concentrations (□ = 0% w/w, ○ = 0.1% w/w, and △ = 0.2% w/w) as a function of deposited tyloxapol mass when delivered on an entangled PA solution subphase.

surfactant masses were achieved by varying both concentration and deposited volume. The range of surfactant masses deposited is comparable to that spanned in Figure 9 for aerosols, but the spread distances are larger. The single microliter drop experiments administer the surfactant in a highly localized region and over a much shorter time interval than the aerosol, which would naturally be dispersed over a larger area over a long period of time, which allows more time for surfactant dissolution into the bulk. Given these effects, the single microliter drop administration likely intensifies the Marangoni effect compared to the aerosol. The qualitatively similar dependence of the maximum spread distance on deposited surfactant mass for both aerosol and single microliter drops is consistent with the pooling of aerosol droplets during the high flux deposition process.

Spreading Behavior on PGM

Aerosol spreading experiments were performed on 5% w/w PGM solutions ($\gamma = 38.3 \pm 3.5$ mN/m at the time of pouring) that mimic the low end of anticipated surface tensions in the conducting airways. Deposited aerosols consisted of aqueous 10 mM fluorescein solutions either without surfactant ($\gamma = 72.2 \pm 0.7$ mN/m) or with 0.4% w/w tyloxapol ($\gamma = 37.0 \pm 1.0$ mN/m) or 1.4% w/w FS-3100 fluorosurfactant ($\gamma = 17.5 \pm 1.0$ mN/m). PGM provides a subphase encompassing more of the complexity of the ASL, and the surfactant-free control and the two surfactant solutions (0.4% w/w tyloxapol and 1.4% w/w FS-3100 fluorosurfactant) provide surface tensions ranging from greater than to less than that of the subphase. When delivered for a total of 55 seconds, the surfactant-free control spread minimally (0.31 ± 0.03 cm), whereas both of the surfactant solutions spread to cover areas three to four times that of the surfactant-free control (tyloxapol: 1.35 ± 0.03 cm ($p < 0.0001$) and FS-3100: 1.06 ± 0.1 cm ($p = 0.02$ by t-test). The two surfactant solutions behaved similarly, $p = 0.11$ for the surfactant comparison.

No significant spreading is observed in the case of surfactant-free aerosol, but surface tension gradients produced upon deposition of surfactant-laden aerosols promote spreading from the deposition region into the neighboring higher surface tension region. These results also demonstrate that, as in the spreading of microliter-scale drops, as long as the surface tension of the formulation in question is lower than that of the subphase, the solution will spread further. This result in conjunction with earlier work on microliter-scale drops indicates that the surfactant-enhanced spreading is dominantly a physical effect and the complex chemistries in the mucus will not qualitatively alter the spreading enhancement.[20,23]

Conclusion

Ultimately, the efficacy of an inhaled medication in obstructive lung disease depends on the ability of the aerosol to adequately reach all areas of the lung. This study and our previous work indicate that surfactants significantly enhance the area covered by post-deposition spreading of aerosolized liquid on an entangled polymer solution subphase.[1,20,23] In this study, we have shown that areas covered by the spreading tracer can be as large as 4.0 cm^2. Large airways have diameters ranging from 0.2–1.2 cm.[28] The significance of the spread areas is readily grasped when one considers that an area of 4.0 cm^2 would correspond to linear distances of approximately 1.2 cm in a cylindrical tube with a diameter of 0.5 cm (i.e., comparable to generation 4). This distance is sufficient to pass through approximately one to two airway generation lengths. Of course, in the lung spreading distances will become more important as one considers spreading relative to mucociliary clearance rates as well.

We can conclude that spreading behavior is a purely physical phenomenon governed only by the lower surface tension of the spreading formulation compared to that of the subphase. There is great uncertainty concerning the surface tension of the ASL. Surface tensions of ASL or pulmonary mucus reported in the literature span a vast range: from 31.9 mN/m to a value that is reported to be greater than that for pure water.[38–40] An endogenous surfactant layer has been described within the airways and surface tension is likely to vary at different locations in the airway tree.[41]

Poly(acrylamide) solutions provide an entangled polymer subphase with a stable surface tension that is comparable to the highest conceivable surface tensions in the airways and that encompasses some key aspects of the ASL. With PGM, some of the biomolecular complexity of ASL is represented, making it potentially a step closer to the real ASL. Two surfactant solutions, tyloxapol and FS-3100 fluorosurfactant with low and extremely low surface tensions, respectively, were used. The surfactant-laden aerosol spreads more than the surfactant-free controls when deposited on either the PA or PGM solution subphase. This enhanced spreading in the case of surfactant-laden aerosol is due to the development of surface tension gradients across the subphase, caused by the presence of surfactant in the aerosol droplets. The developed surface tension gradients induce Marangoni flows along the liquid/vapor interface causing the entire aerosol field to convect across the subphase. No convective spreading is observed for the surfactant-free aerosol field on either of the

subphase because of the absence of Marangoni flows along the subphase surface.

With this study and our previous work performed with a wide variety of surfactant/subphase systems, it can be concluded that as long as the surfactant solution has a lower surface tension than the aqueous ASL mimic subphase, the solution will spread more than a surfactant-free control.[1,20,23] Although aerosol spreading experiments in this study are performed with tyloxapol and FS-3100 fluorosurfactant, similar qualitative spreading behavior has been observed for different surfactant systems (anionic, cationic, and nonionic) for aerosol[1] as well as microliter scale drops[20] on similar subphases. Our studies demonstrate that the total delivered surfactant mass is the best predictor of the maximum extent of spreading, and that at high fluxes, the delivered aerosol spreads as a coalesced mass, instead of an agglomeration of unfused droplets. Ultimately, given the complex nature of surface conditions within the lungs, *in vivo* studies will need to be performed to validate these *in vitro* findings.

Acknowledgments

The material is based on work supported in part by National Science Foundation under grants CBET-0931057 and in part by the National Heart, Lung and Blood Institute at National Institutes of Health under grant number R01 HL105470. The authors would like to thank C. Dipietro for the measurements shown in Figure 3, Prof. S. Tristram-Nagle for the use of the Anton-Paar DMA 5000M scanning densimeter in her laboratory, and A. Stetten for the density measurements. The authors would also like to thank G. Dunér, A. Stetten, and Y. Zhang for discussions relating to the subject matter presented. The contents of this article are solely the responsibility of the authors and do not necessarily represent the official views of NHLBI.

Author Disclosure Statement

The authors declare that no competing financial interests exist.

References

1. Marcinkowski AL, Garoff S, Tilton RD, Pilewski JM, and Corcoran TE. Postdeposition dispersion of aerosol medications using surfactant carriers. J Aerosol Med Pulm Drug Deliv. 2008;21:361–370.
2. Brown JS, Zeman KL, and Bennett WD. Regional deposition of coarse particles and ventilation distribution in healthy subjects and patients with cystic fibrosis. J Aerosol Med. 2001;14:443–454.
3. Smaldone GC, and Palmer LB. Aerosolized antibiotics: Current and future. Respir Care. 2000;45:667–675.
4. Svartengren K, Lindestad PA, Svartengren M, Bylin G, Philipson K, and Camner P. Deposition of inhaled particles in the mouth and throat of asthmatic subjects. Eur Respir J Off J Eur Soc Clin Respir Physiol. 1994;7:1467–1473.
5. De Backer W, Devolder A, Poli G, Acerbi D, Monno R, Herpich C, Sommerer K, Meyer T, and Mariotti F. Lung deposition of BDP/formoterol HFA pMDI in healthy volunteers, asthmatic, and COPD patients. J Aerosol Med Pulm Drug Deliv. 2010;23:137–148.
6. Ruddy J, Emerson J, Moss R, Genatossio A, McNamara S, Burns JL, Anderson G, and Rosenfeld M. Sputum tobramycin concentrations in cystic fibrosis patients with repeated administration of inhaled tobramycin. J Aerosol Med Pulm Drug Deliv. 2013;26:69–75.
7. Corcoran TE. Inhaled delivery of aerosolized cyclosporine. Adv Drug Deliv Rev. 2006;58:1119–1127.
8. Ramsey BW, Pepe MS, Quan JM, Otto KL, Montgomery AB, Williams-Warren J, Vasiljev KM, Borowitz D, Bowman CM, Marshall BC, Marshall S, and Smith AL. Intermittent administration of inhaled tobramycin in patients with cystic fibrosis. Cystic Fibrosis Inhaled Tobramycin Study Group. N Engl J Med. 1999;340:23–30.
9. Fiel SB. Aerosolized antibiotics in cystic fibrosis: Current and future trends. Expert Rev Respir Med. 2008;2:479–487.
10. Merlo CA, Boyle MP, Diener-West M, Marshall BC, Goss CH, and Lechtzin N. Incidence and risk factors for multiple antibiotic-resistant Pseudomonas aeruginosa in cystic fibrosis. Chest. 2007;132:562–568.
11. Geller DE, Pitlick WH, Nardella PA, Tracewell WG, and Ramsey BW. Pharmacokinetics and bioavailability of aerosolized tobramycin in cystic fibrosis. Chest. 2002;122:219–226.
12. Berg JC. *An Introduction to Interfaces and Colloids: The Bridge to Nanoscience.* Singapore: World Scientific Publishing; 2010.
13. Bertram CD, and Gaver DP. Bio-fluid mechanics of the pulmonary system. Ann Biomed Eng. 2005;33:1681–1688.
14. Grotberg JB. Respiratory fluid mechanics and transport processes. Annu Rev Biomed Eng. 2001;3:421–457.
15. Grotberg JB, and Gaver III DP. A synopsis of surfactant spreading research. J Colloid Interface Sci. 1996;178:377–378.
16. Nimmo AJ, Carstairs JR, Patole SK, Whitehall J, Davidson K, and Vink R. Intratracheal administration of glucocorticoids using surfactant as a vehicle. Clin Exp Pharmacol Physiol. 2002;29:661–665.
17. Van 't Veen A, Gommers D, Mouton JW, Kluytmans JA, Krijt EJ, and Lachmann B. Exogenous pulmonary surfactant as a drug delivering agent: Influence of antibiotics on surfactant activity. Br J Pharmacol. 1996;118:593–598.
18. Grotberg JB, Halpern D, and Jensen OE. Interaction of exogenous and endogenous surfactant: Spreading-rate effects. J Appl Physiol. 1995;78:750–756.
19. Halpern D, Jensen OE, and Grotberg JB. A theoretical study of surfactant and liquid delivery into the lung. J Appl Physiol. 1998;85:333–352.
20. Koch K, Dew B, Corcoran TE, Przybycien TM, Tilton RD, and Garoff S. Surface tension gradient driven spreading on aqueous mucin solutions: A possible route to enhanced pulmonary drug delivery. Mol Pharm. 2011;8:387–394.
21. Afsar-Siddiqui AB, Luckham PF, and Matar OK. The spreading of surfactant solutions on thin liquid films. Adv Colloid Interface Sci. 2003;106:183–236.
22. Starov V. On the spreading of an insoluble surfactant over a thin viscous liquid layer. J Colloid Interface Sci. 1997;190:104–113.
23. Sharma R, Corcoran TE, Garoff S, Przybycien TM, Swanson ER, and Tilton RD. Quasi-immiscible spreading of aqueous surfactant solutions on entangled aqueous polymer solution subphases. ACS Appl Mater Interfaces. 2013;5:5542–5549.
24. Lee KS, and Starov VM. Spreading of surfactant solutions over thin aqueous layers at low concentrations: Influence of solubility. J Colloid Interface Sci. 2009;329:361–365.

25. Petitjeans P. A surface tension for miscible fluids. Comptes Rendus L Acad Des Sci Ser Ii Fasc B-Mecanique Phys Chim Astron. 1996;322:673–679.
26. Liu Y, Lipowsky R, and Dimova R. Concentration dependence of the interfacial tension for aqueous two-phase polymer solutions of dextran and polyethylene glycol. Langmuir. 2012;28:3831–3839.
27. Jensen OE, and Grotberg JB. Insoluble surfactant spreading on a thin viscous film: Shock evolution and film rupture. J Fluid Mech. 1992;240:259. doi:10.1017/S0022112092000090.
28. Weibel ER, and Gomez DM. Architecture of the human lung: Use of quantitative methods establishes fundamental relations between size and number of lung structures. Sci. 1962;137:577–585.
29. Finlay WH. Particle deposition in the respiratory tract. In: *The Mechanics of Inhaled Pharmaceutical Aerosols: An Introduction.* Academic Press; 2001:119–174.
30. Chan TL, and Lippmann M. Experimental measurements and empirical modelling of the regional deposition of inhaled particles in humans. Am Ind Hyg Assoc J. 1980;41: 399–409.
31. Heyder J, and Gebhart J. Gravitational deposition of particles from laminar aerosol flow through inclined circular tubes. J Aerosol Sci. 1977;8:289–295.
32. Zhu Y, Xu G, Xin X, Zhang H, and Shi X. Surface tension and dilational viscoelasticity of water in the presence of surfactants tyloxapol and Triton X-100 with cetyl trimethylammonium bromide at 25°C. J Chem Eng Data. 2009; 54:989–995.
33. Gaver DP, and Grotberg JB. Droplet spreading on a thin viscous film. J Fluid Mech. 1992;235:399.
34. Sjöback R, Nygren J, and Kubista M. Absorption and fluorescence properties of fluorescein. Spectrochim Acta Part A Mol Biomol Spectrosc. 1995;51:L7–L21.
35. Van Nierop EA, Ajdari A, and Stone HA. Reactive spreading and recoil of oil on water. Phys Fluids. 2006;18: 038105.
36. Karapetsas G, Craster RV, and Matar OK. Surfactant-driven dynamics of liquid lenses. Phys Fluids. 2011;23:122106.
37. Zar JH. Biostatistical analysis. Pearson Education. New Jersey; 2010;435.
38. Im Hof V, Gehr P, Gerber V, Lee MM, and Schurch S. In vivo determination of surface tension in the horse trachea and in vitro model studies. Respir Physiol. 1997; 109:81–93.
39. Kirkness JP, Christenson HK, Garlick SR, Parikh R, Kairaitis K, Wheatley JR, and Amsi TC. Decreased surface tension of upper airway mucosal lining liquid increases upper airway patency in anaesthetised rabbits. J Physiol. 2003;547:603–611.
40. Albers GM, Tomkiewicz RP, May MK, Ramirez OE, and Rubin BK. Ring distraction technique for measuring surface tension of sputum: Relationship to sputum clearability. J Appl Physiol. 1996;81:2690–2695.
41. Geiser M, Schurch S, and Gehr P. Influence of surface chemistry and topography of particles on their immersion into the lung's surface-lining layer. J Appl Physiol. 2003; 94:1793–1801.

Received on July 18, 2014
in final form, January 13, 2015

Reviewed by:
Peter Gehr
Jung Soo Suk

Address correspondence to:
Stephen Garoff, PhD
Department of Physics
Carnegie Mellon University
5000 Forbes University
Pittsburgh, PA 15213

E-mail: sg2e@andrew.cmu.edu